Supplementary Information for

Intelligent soliton molecules control in an ultrafast thulium fiber laser

Yi Zhou,[a,*] Kangwen Yang,[a,b,c] Kevin K. Tsia,[a,b] Heping Zeng,[d] and Kenneth K. Y. Wong [a,b]

[a]The University of Hong Kong, Department of Electrical and Electronic Engineering, Hong Kong, China

[b]Advanced Biomedical Instrumentation Centre, Hong Kong Science Park, Shatin, New Territories, Hong Kong, China

[c]University of Shanghai for Science and Technology, Shanghai Key Laboratory of Modern Optical System, and Engineering Research Center of Optical Instrument and System, Ministry of Education, School of Optical Electrical and Computer Engineering, Shanghai 200093, China

[d]East China Normal University, State Key Laboratory of Precision Spectroscopy, Shanghai 200062, China

[*] *Corresponding author*
Email: zhouyi08@hku.hk
Email: kywong@eee.hku.hk

Contents

Section 1. Single-shot spectra of doublet and triplet SM in one pulsation period during switching

The maximal and minimal spectrum extents within a pulsation period of doublet and triplet SM during switching are shown in Fig. S1, corresponding to Figs. 2b and 2o of the main text. Small spectra amplitude variation can be observed during one pulsation period of 6 RT (Fig. S1a), evidence the doublet SM with a weak pulsation ratio. Further, obvious spectra amplitude variation can be resolved during one pulsation period in Figs. S1b and S1c, verify the triplet SM with a moderate pulsation ratio during switching. The pulsation periods are 6 RT for both the before and after switching processes. The inset in Figs. S1b and S1c reflect the different inter-soliton temporal separations of triplet SM, which is consistent with the spectra features during switching.

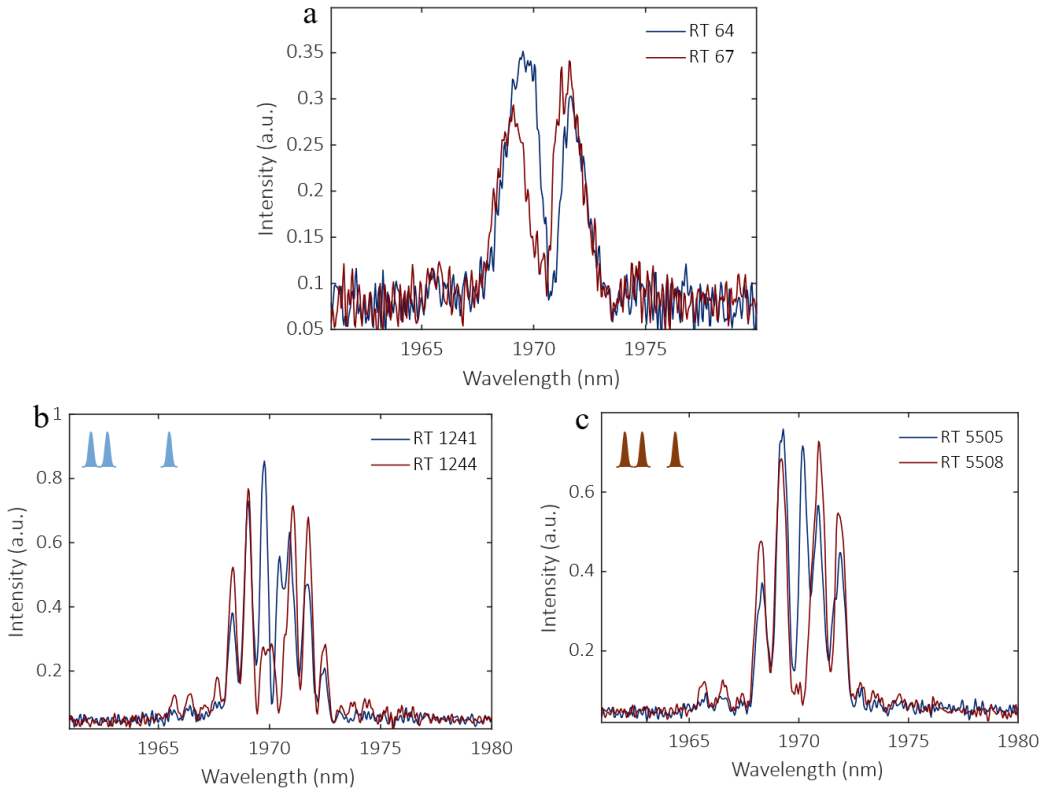

Fig. S1. Single-shot spectra of maximal and minimal spectrum extents within a pulsation period. (a) Pulsation doublet SM before switching. (b) Pulsation triplet SM before switching. (c) Pulsation triplet SM after switching.

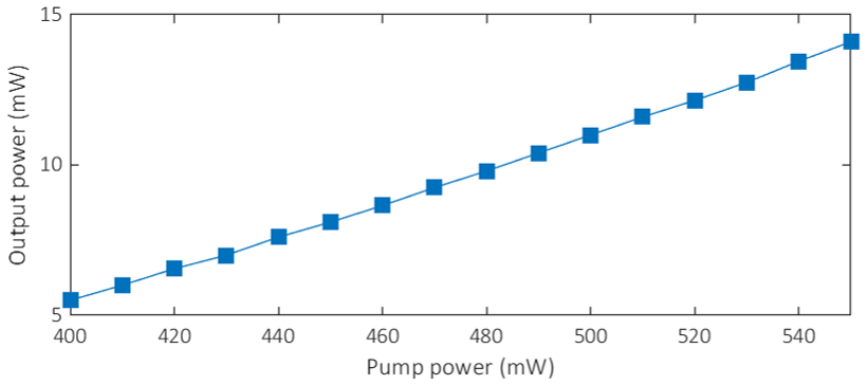

Fig. S2. Output power of pulse with the increased pump power.

Section 2. Internal motion of doublet and triplet SM during switching

As the ultrafast lasers carve each pulse profile similarly in SMs, the most relevant internal variables are the relative phases and temporal separations among solitons. The temporal separation and relative phase evolution of doublet SM during switching are shown in Figs. S3a and S3b. The inter-soliton separation of SM experiences dramatic variation during switching corresponding to multiple repulsive and attractive interactions (Fig. S3a), and maintains a constant value after the transition to a station state corresponding to a larger temporal interval compared to the initial pulsation state (from 4.28 ps to 6.73 ps). The rapid oscillation phase evolution (see the inset of Fig. S3b) with a period of ~6 RT is consistent with the SM pulsation operation. In contrast, the relative phase of SM after switching is a stationary relation and verified in the inset of Fig. S3b. The trajectory of (τ, φ) shown in Fig. S3c indicates the trace evolves on the fixed orbits before and after switching, while experiencing intricate evolution during the intermediate transition state (RT 2080-2780 in Fig. S3c).

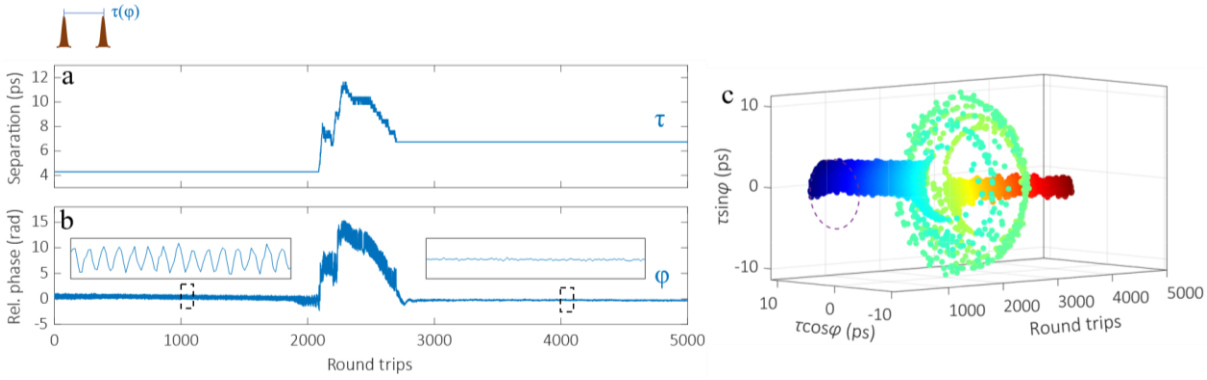

Fig. S3. Retrieved temporal separation and relative phase of the doublet SM during switching. (a) temporal separation, (b) relative phase, (c) trajectories of (τ, φ) in the interaction space.

Similarly, the temporal separation and relative phase of pulsation triplet SM during switching are shown in Figs. S4a and S4b. The temporal interval between leading and middle solitons (τ_{12}) keeps fixed of 4.4 ps during switching. While the triple soliton has a fast decrease in the temporal separation compared to the leading and middle solitons, as verified by the temporal trace evolution (τ_{13} from 18.83 ps decrease to 14.43 ps). Intriguingly, the relative phase evolution (φ_{12} and φ_{13}) are both characterized by rapid oscillation with a period of ~ 6 RT, consistent with the pulsation SM operation (inset in Fig. S4b). The difference of the SM after switching is the rapid relative phase oscillation modulated by a slowly varying envelope with a period of ~64 RT, and this feature does not exist for the before-switching state. The trajectories evolution of (τ_{12}, φ_{12}) and (τ_{13}, φ_{13}) are shown in Figs. S4d and S4c. The 3D interaction (Fig. S4d) indicates (τ_{12}, φ_{12}) evolve on the fixed orbit with temporal separation of 4.4 ps. While the trajectories of (τ_{13}, φ_{13}) evolve along two orbits with two different temporal separations of 18.83 ps and 14.43 ps, corresponding to before and after switching states. Among them, the multiple turning points of phase evolution (RT 2500 to 2920 in Fig. S4c) correspond to the sliding phase, consistent with the relative phase evolution in Fig. S4b.

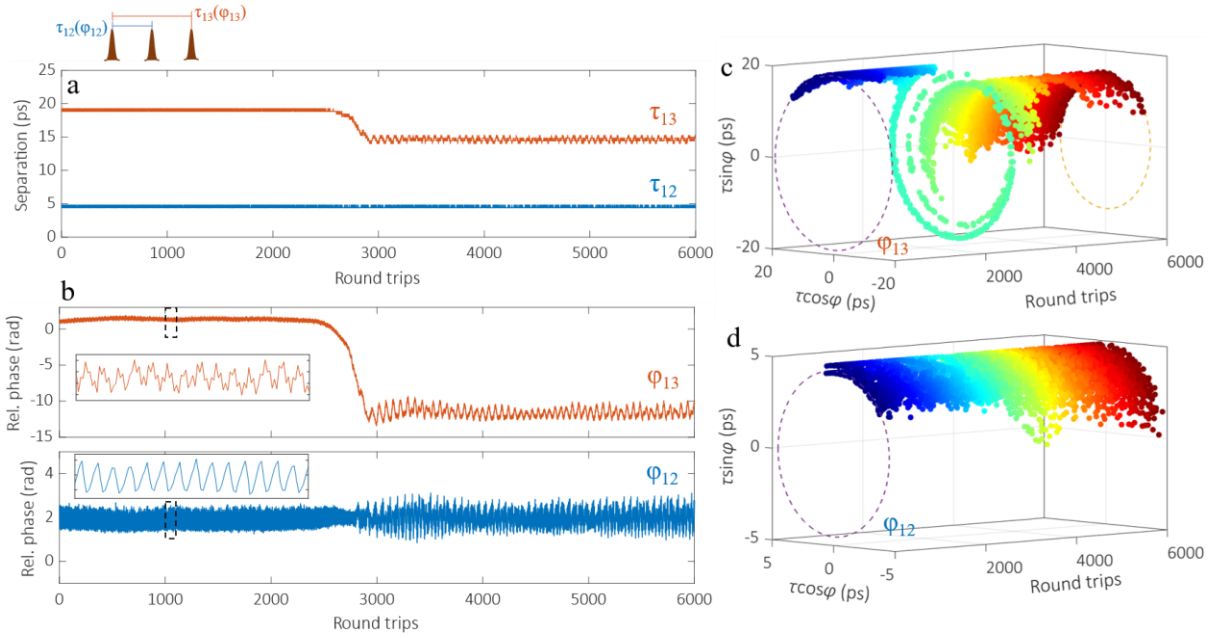

Fig. S4. Retrieved temporal separations and relative phases of the triplet SM during switching. (a) Temporal separation and (b) relative phase. (c) Trajectories of (τ_{13}, φ_{13}) in the interaction space. (d) Trajectories of (τ_{12}, φ_{12}) in the interaction space.

Section 3. Numerical simulation of SM switching

In the experiment, SM switching can be precisely manipulated by changing the optimized drive voltage of EPC. To support and better interpret the physical mechanism of the switching dynamics, numerical simulations of doublet and triplet SM switching are executed. During the simulation, we first generate a stable pulsation SM (Figs. S5a and S5b). Then, changing the parameter of SA to $E_s = 6$ pJ, $\Delta R = 0.3$, $P_0 = 35$ W, the doublet SM switching from pulsation to stationary state can be observed, corresponding to an increase in inter-soliton temporal separation after state transformation (Figs. S5e and S5f). The simulated single-shot spectral and continuous spectra evolution qualitatively agree well with the experiment observation (Figs. 2a-2h), verifying the different SM operation states before and after switching (Figs. S5a-S5d).

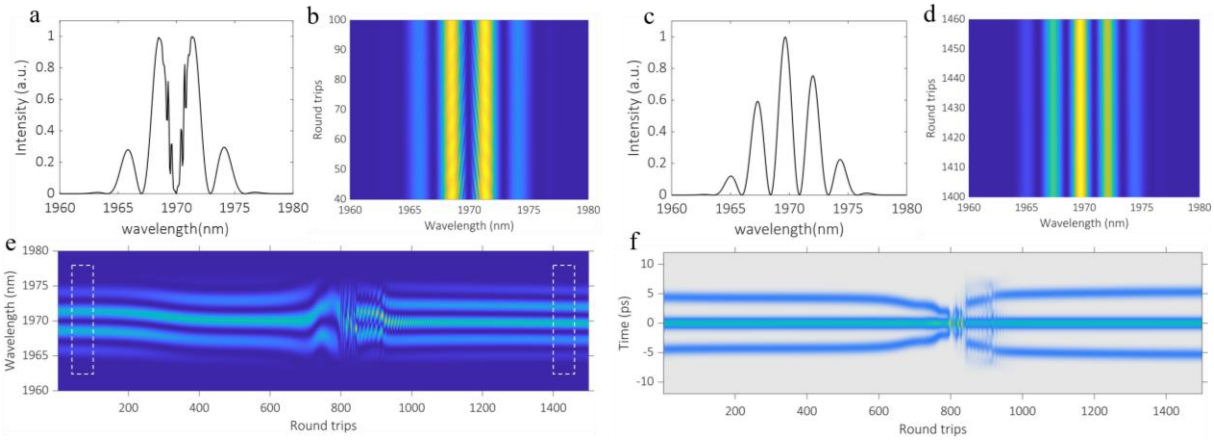

Fig. S5. Numerical simulations of the doublet SM switching. (a) Single-shot spectrum and (b) zoom-in plot of spectra evolution before switching. (c) Single-shot spectrum and (d) zoom-in plot of spectra evolution after switching. (e)

Simulated spectra and (f) autocorrelation trace evolution of doublet SM during switching.

Similarly, we first generate a stable pulsation triplet SM, and varying the parameter of SA to E_s = 6.2 pJ, $\Delta R = 0.1$, $P_0 = 20$ W, the pulsation triplet SM switching with different temporal intervals can be resolved (Figs. S6e and S6f). During switching, the leading and middle solitons keep a fixed temporal separation, while maintaining a constant attractive interaction with the trailing soliton, thereby leading to a decreasing temporal interval and sliding phase evolution between the leading and trailing pulses. The simulated single-shot and continuous spectral evolution (Figs. S6a-S6d) reproduced the experiment results convincingly (Figs. 2i-2p). These numerical simulations provide theoretical support for the programmable drive voltage of EPC corresponding to altering the nonlinear transfer function in the laser, thereby achieving flexible and precise manipulation of SM operation in different states.

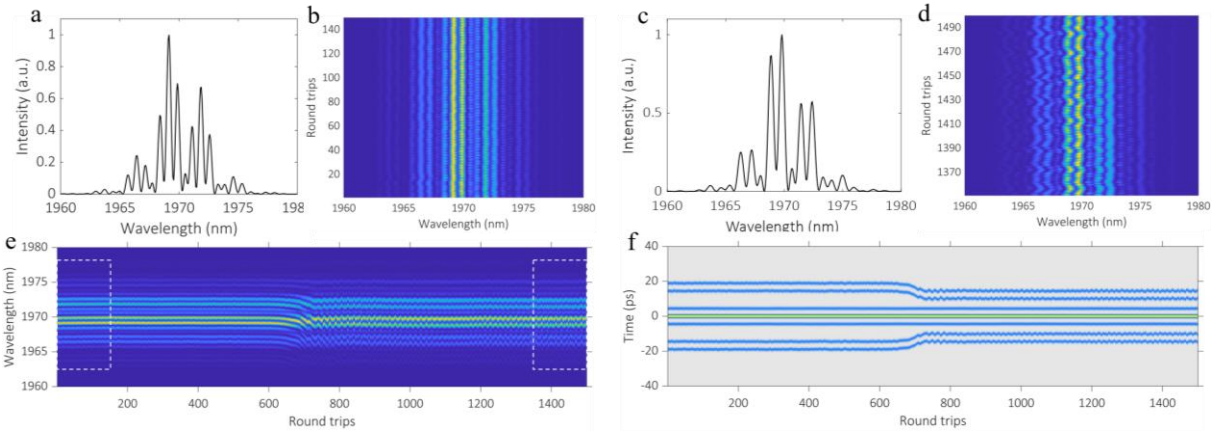

Fig. S6. Numerical simulations of the triplet SM switching. (a) Single-shot spectrum and (b) zoom-in plot of spectra evolution before switching. (c) Single-shot spectrum and (d) zoom-in plot of spectra evolution after switching. (e) Simulated spectra and (f) autocorrelation trace evolution of triplet SM during switching.

Section 4. RF spectrum of SM with stationary operation and pulsation frequency locking

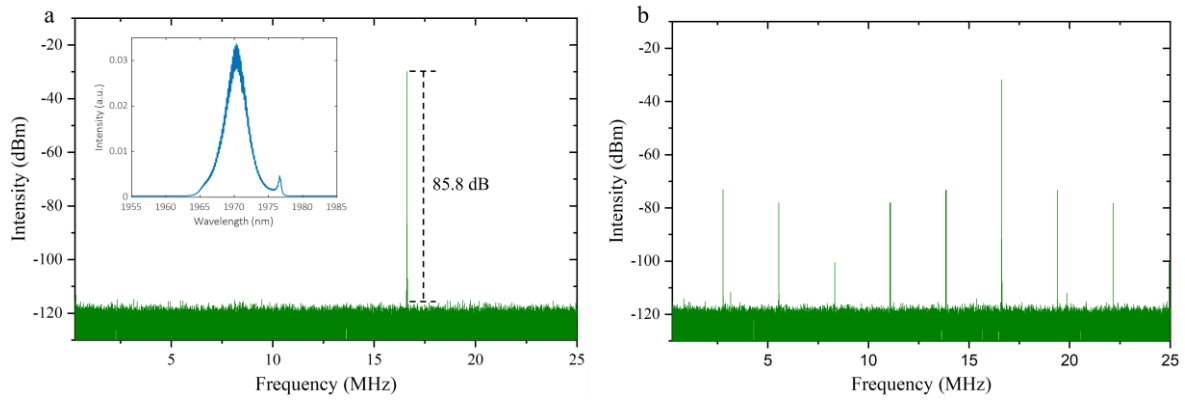

Fig. S7. (a) RF spectrum of stationary soliton molecule. The inset corresponds to the optical spectra of stationary SM. (b) RF spectrum of SM with pulsation frequency locking.

During EA optimization in the experiment, the RF spectrum is calculated through fast Fourier transform of the laser intensity recorded by the oscilloscope. The relatively low SNR of the calculated RF spectrum is owing to the limited sampling points recorded by the oscilloscope. Whereas the calculated RF spectrum in Figs. 3c and 3d can still verify the pulsation SM generation with the characteristic RF sideband. Further, we measure the RF spectrum of a stationary SM through the radio spectrum analyzer (Fig. S7a), and the 85.8 dB SNR demonstrates the good stability of our mode-locked laser.

Further, the pulsation period = $f_r/|f_{\pm 1} - f_r|$, the fundamental frequency of 16.6225 MHz (f_r) and the sideband frequency of 13.8521 MHz (f_{-1}) shown in Fig. 3c demonstrates the integer multiple relationships (pulsation period of 6 RT) and reflects the pulsation frequency locking (PFL) of SM. We also remeasure the RF spectrum of optimized SM through the radio spectrum analyzer shown in Fig. S7b, which reflects the integer multiple relationships well (pulsation period of 6 RT) and further demonstrates the PFL characteristic of SM.

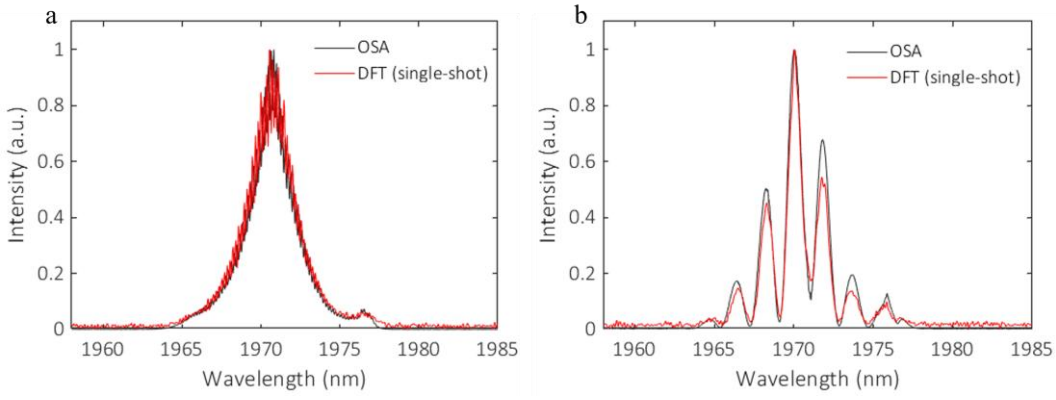

Fig. S8. The good agreement between the spectra measured by OSA (black) and the single-shot DFT spectrum (red) of (a) large pulsation ratio and (b) small pulsation ratio, corresponding to Figs. 4i and 4c, respectively.

In the experiment, the DFT branch was composed of a CFBG with 300 ps/nm dispersion, and the output signal was detected by a 12.5 GHz photodiode, corresponding to the DFT spectral resolution of 0.29 nm. To verify the DFT spectra resolution is sufficient to discern the detailed spectral evolution and

the corresponding autocorrelation evolution derived from the spectra in Figs. 4 and 5, the spectra measured by OSA (black) and the single-shot DFT spectrum (red) of large and small pulsation ratios (corresponding to Figs. 4i and 4c) are shown in Fig. S8. The good agreement between the spectra measured by OSA with 0.05 nm resolution and the single-shot DFT spectrum further demonstrates the DFT spectra resolution is sufficient to resolve the detailed spectral and corresponding autocorrelation evolution.

Section 5. (2+1) SMC with tunable pulsation ratio and triplet pulsation SM

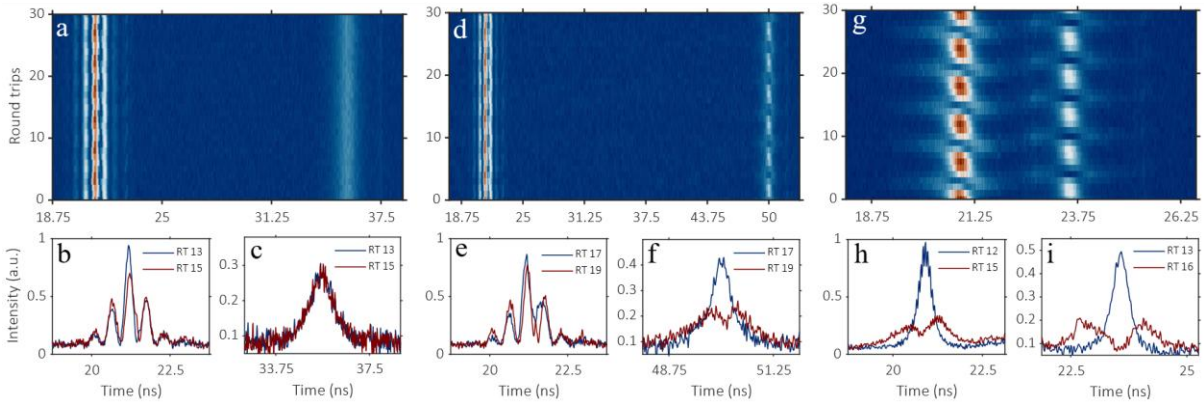

Fig. S9. Evolutionary algorithm optimization results for (2+1) SMC with a tunable pulsation ratio. Dynamics of (2+1) SMC with (a-c) small, (d-f) moderate, and (g-i) large pulsation ratio. (a, d, g) DFT spectral evolution over consecutive cavity RTs. (b, c, e, f, h, i) Single-shot spectra of maximal and minimal spectrum extents within a pulsation period.

In the experiment, the (2+1) soliton molecular complexes (SMC), consisting of one soliton pair molecule and a soliton singlet with nanosecond temporal separation, can be generated in the fiber laser at a pump power of 440 mW. Utilizing the EA and defined fitness function, (2+1) SMC with tunable pulsation ratios can also be realized. The DFT spectra and field autocorrelation trace evolution are shown in Fig. S9. The weakest pulsation operation of SMC is shown in Figs. S9a-S9c, and the moderate and strongest pulsation ratio of SMC are shown in Figs. S9d-S9f and S9g-S9i, respectively. The discrepancy in pulsation ratio of the three types of SMC can be further resolved in the single-shot spectra of maximal and minimal spectrum extents within a pulsation period. The spectra variation of the leading soliton pair molecule in a pulsation period is small (Fig. S9b) and the trailing soliton singlet depicts a stationary operation (Fig. S9c), demonstrating the weakest pulsation operation. In contrast, the spectra in Figs. S9e and S9f have a stronger pulsation ratio compared to the weakest pulsation state (Figs. S9a-s9c). Especially, the trailing soliton singlet (Fig. S9f) has a more obvious spectra amplitude variation compared to Fig. S9c. Further, the peak-to-dip flip characteristic in spectra can both be observed in the leading soliton pair molecule and trailing single soliton (Figs. S9h and S9i), demonstrating the SMC with the strongest pulsation ratio. Notably, the leading and trailing solitons have the same pulsation period in the moderate and strongest pulsation operation, while the leading soliton molecule has a lag synchronization ~ 1 RT compared to the trailing soliton singlet in the strongest pulsation ratio (Figs.S9g-S9i).

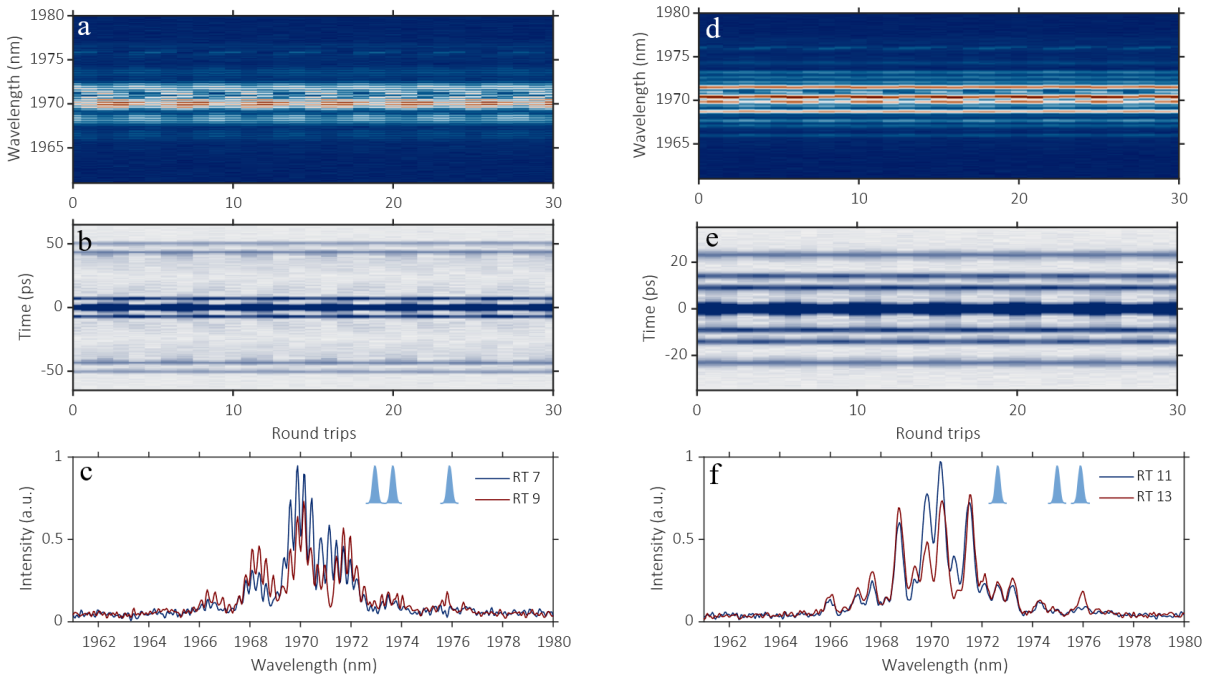

Fig. S10. Triplet pulsation SM with different operation states. (a, d) DFT spectral evolution over consecutive cavity RTs. (b, c) Field autocorrelation trace evolution over consecutive cavity RTs. (c, f) Single-shot spectra of maximal and minimal spectrum extents within a pulsation period.

Further, the triplet SM with picosecond inter-soliton temporal separation and weak pulsation ratio can also be observed in the laser output. The DFT spectra and field autocorrelation trace evolution of two types of triplet pulsation SM are shown in Fig. S10a, S10b, S10d, S10e. The different soliton temporal distribution in SMs is consistent with the distinct spectra features. Small amplitude variations of the single-shot spectra within a pulsation period (Figs. S10c and S10f) reflect the weak pulsation ratio of these two types of triplet SM.

Section 6. Optical spectra of SMs with different operation states during continuous switching

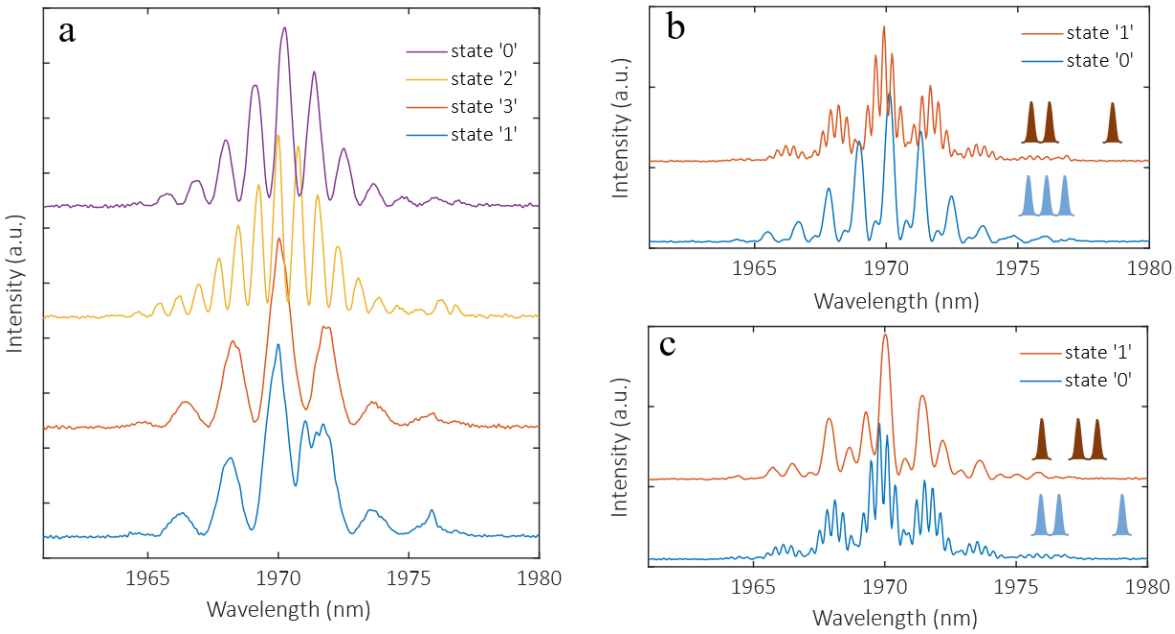

Fig. S11. Optical spectra of doublet and triplet SM with different operation states during continuous switching. (a) Optical spectra of doublet SM with four different states during switching. (b, c) Optical spectra of triplet SM with two operation states during switching.

The multiple characteristics of SMs, e.g., stationary or pulsation state, and inter-soliton temporal separation, are determined by the spectra features. The optical spectra of doublet SM with four operation states during continuous switching are shown in Fig. S11a corresponding to Figs. 6g and 7 of the main text, including SM with weak (state '3') and moderate pulsation ratio (state '1'), stationary SM with large (state '2') and small (state '0') inter-soliton temporal interval. Moreover, the optical spectra of triplet stationary SM with two operation states during continuous switching are shown in Figs. S11b and S11c, corresponding to Figs. 6i and 6k of the main text. The inter-solion temporal separation is consistent with the spectra pattern features.

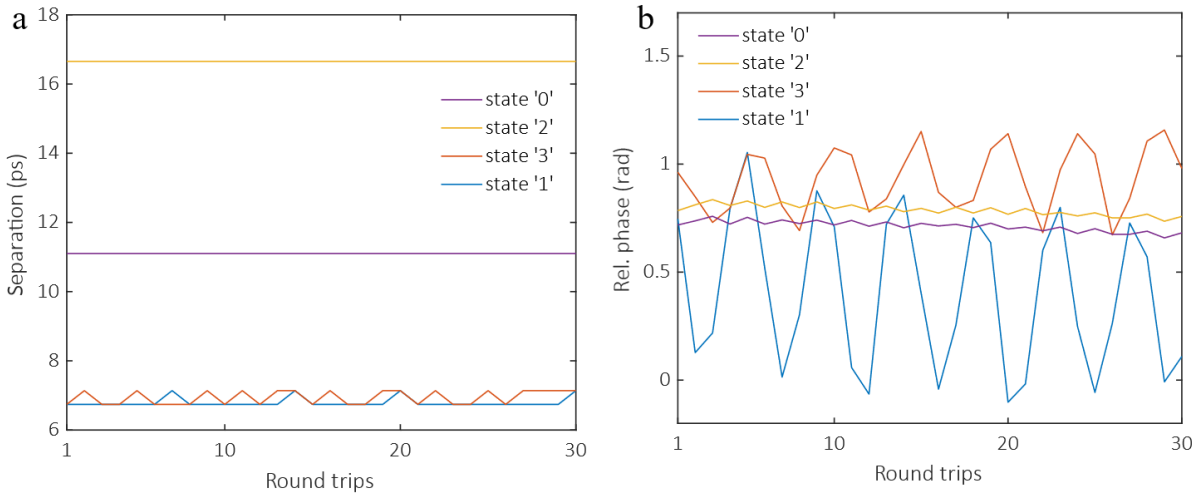

Fig. S12. (a) Temporal separation and (b) relative phase of doublet SM with different operation states during continuous switching.

The temporal separation and relative phase (Fig. S12) further indicate the doublet SM operates in four different states. The SM of state '0' and '2' with stationary relative phase evolution suggest remarkably different inter-soliton temporal separations (11 ps for state '0' and 16.7 ps for state '2'). Parallelly, the SM of state '1' and '3' have almost the same inter-soliton separation of 6.7 ps, while the relative phase oscillation amplitude of state '1' is more than three times compared to state '3'. Therefore, the obvious different features of the four SM operation states can be utilized to achieve digital quaternary encoding in this platform by programming the drive voltage of EPC.

Section 7. Reproducibility and stability of SM with the application of EPC

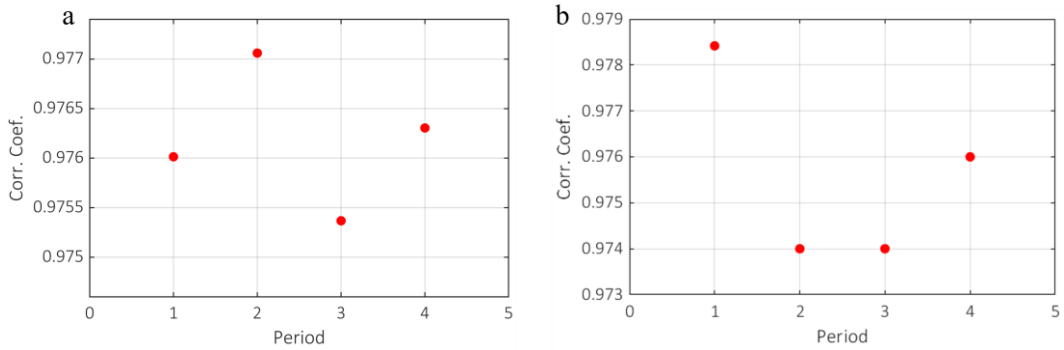

Fig. S13. Pearson correlation coefficient between the first period DFT spectral and the following harnessing periods. (a) Continuous switching of stationary SM corresponds to Fig. 6a. (b) Continuous switching of SM between pulsation and stationary state corresponds to Fig. 6c.

Quantifying the reproducibility and stability of the SM with the application of EPC is also of considerable importance. To verify the reproducibility of soliton molecule consecutive switching with EPC, we calculate the Pearson correlation coefficient between the first-period DFT spectra and the following harnessing periods. For the five-period consecutive switching of SM between two states (Figs. 6a and 6c), the calculated correlation coefficient results (Figs. S13a and S13b) further validate the high reproducibility of the soliton molecule switching with EPC.

We also measured the stability of optical spectra of two pulsation SM states after fixing the drive voltage of EPC, as shown in Figs. S14a and S14b. The optical spectra are very stable during the measurement, demonstrating high stability over time after the application of EPC.

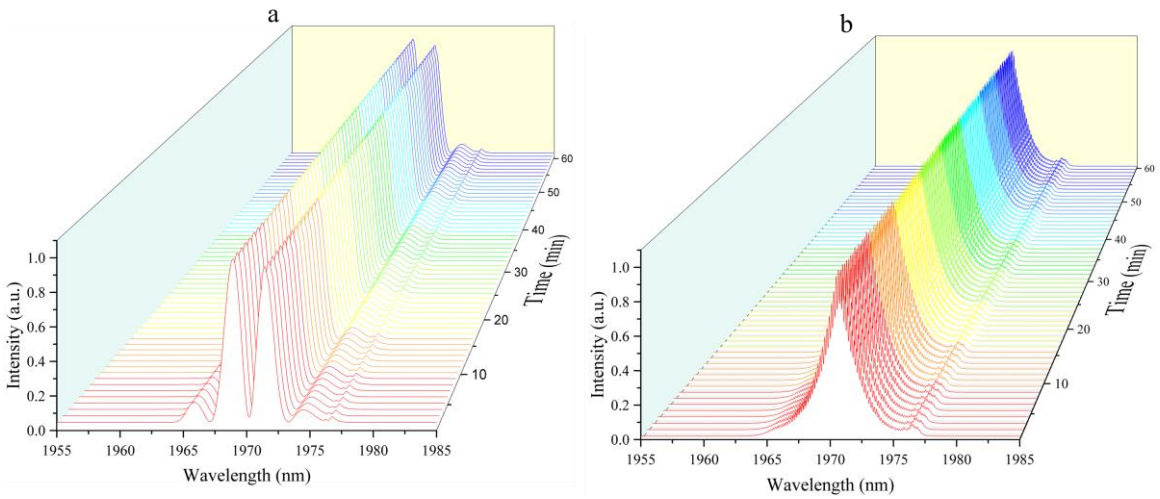

Fig. S14. (a) and (b) Optical spectra of pulsation SM within 60 minutes, corresponding to the pulsation SM in Figs. 2a and 4i.

Section 8. Key devices used in the mode-locked fiber laser

For the convenience of other groups in the field to build a fiber laser with the same or similar structure to our work, we list the model number of key components in Table S1.

Table S1 Key devices used in the mode-locked fiber laser

Symbol	Description	Model number
FBG	Fiber Bragg grating	TeraXion PSR-1970-30-0S1-0L
EPC	Electronic polarization controller	General Photonics Mini Dynamic Polarization Controller - PolaRITE™ III (MPC-3X)
Filter	Spectra bandpass filter	Advanced Fiber Resources BP-1970-6-2-L-1-1
WDM	Wavelength division multiplexer	Advanced Fiber Resources WDM-1-15701970-2-L-1-6
OC	30:70 fiber optic coupler	Advanced Fiber Resources SMC-1-1970-30-2-L-Q-6
Isolator	Polarization-dependent isolator	Advanced Fiber Resources PDI-2000-1-L-Q-F-5
TDF	Thulium-doped fiber	Nufern TSF-9-125
SMF	Single-mode fiber	Corning SMF-28e
Pump diode	1.5 μm CW Fiber Laser	Connet Laser Technology VFLS-1570-B/M-MP